


**Suppression of long-range ferromagnetic order in the  $\text{Ce}_x\text{La}_{1-x}\text{TiGe}_3$  system**

Jeonghun Lee, Anja Rabus, C. Coutts, and Eundeok Mun

*Department of Physics, Simon Fraser University, Burnaby, British Columbia, Canada V5A 1S6* (Received 16 October 2018; revised manuscript received 14 December 2018; published 23 January 2019)

We report specific heat, magnetization, and resistivity measurements on single crystals of  $\text{Ce}_x\text{La}_{1-x}\text{TiGe}_3$  systems. When the Ce concentration  $x$  is increased, the system changes from a single-ion Kondo system for  $x = 0.05$  into a ferromagnetic Kondo lattice for  $x = 1$ , where the magnetic part of electrical resistivity reveals a single-ion scaling with  $x$ . The isoelectric substitution of Ce by La atoms causes a change of the relative strength of competing energy scales of Kondo and RKKY interaction and crystalline electric field (CEF). The substitutions induce the continuous evolution of the Kondo temperature  $T_K$  and the linear variation of ferromagnetic ordering temperature  $T_c$ , which are accompanied by a change of the CEF level scheme of the Ce ions. The composition-temperature ( $x$ - $T$ ) phase diagram for  $\text{Ce}_x\text{La}_{1-x}\text{TiGe}_3$  is constructed by a combination of magnetization, specific heat, and resistivity measurements. The ferromagnetic ordering temperature is linearly suppressed as  $x$  decreases and vanishes near the critical concentration  $x_c = 0.1$ , but conventional quantum criticality is absent near  $x_c$ . The specific heat measurement for  $x = 0.05$  reveals the power law increase of the electronic specific heat coefficient  $C_m/T \propto 1/T$  with a large value of  $\sim 3.5$  J/mol K<sup>2</sup> at  $T = 0.4$  K. The magnetic susceptibility for  $x = 0.05$  also shows a power law dependence  $\chi(T) \propto 1/T$  below 10 K.

DOI: [10.1103/PhysRevB.99.045135](https://doi.org/10.1103/PhysRevB.99.045135)**I. INTRODUCTION**

The heavy fermion (HF) compounds are the canonical example of strongly correlated electron systems and are the prototypical system in which to study competing ground states [1]. Competition between the Kondo effect and long-range magnetic interactions leads to the well-known Doniach diagram [2], giving a good description of quantum phase transitions in many heavy-fermion compounds [3–5]. The quantum critical point (QCP), which separates the ground states between the magnetically ordered state and paramagnetic state, can be reached by nonthermal control parameters such as pressure, substitution, and magnetic field. Quantum phase transitions continue to be a central topic in condensed matter physics because they are responsible for a variety of unconventional low temperature phenomena [6]. To date, most of the theoretical and experimental investigations for the quantum phase transition have focused on antiferromagnetic (AFM) HF metals [7,8]. The spin fluctuations associated with the quantum phase transitions can lead to non-Fermi liquid behavior in metals and even induce novel phases of matter [4]. There are many examples of AFM systems [3] where the Kondo effect coexists with the Ruderman-Kittel-Kasuya-Yosida (RKKY) interaction, whereas ferromagnetic (FM) Kondo lattice systems are relatively rare [9]. Although the number of known FM HF materials, e.g., CePt [10], CeAgSb<sub>2</sub> [11], CePdSb [12], CeTiGe<sub>3</sub> [13], YbPdSi [14], YbNi<sub>4</sub>P<sub>2</sub> [15], UGe<sub>2</sub> [16], U<sub>3</sub>P<sub>4</sub> [17], and URhGe [18] is increasing gradually; the FM quantum criticality has been studied less [9]. The FM ordering can be suppressed by doping or pressure, often leading to various phase diagrams including the tricritical wings [19], quantum Griffiths phase [20,21], or non-Fermi liquid behavior [22]. Several theories have been proposed to explain these intriguing phenomena [9].

The purpose of this work is an investigation of the competing energy scales between the RKKY intersite interaction that leads to a FM ordering and the Kondo effect resulting in a suppression of local moments in the HF  $\text{Ce}_x\text{La}_{1-x}\text{TiGe}_3$  system. The CeTiGe<sub>3</sub> compound crystallizes in the hexagonal BaNiO<sub>3</sub>-type structure (space group 194,  $P6_3/mmc$ ) [13,23]. At ambient pressure, CeTiGe<sub>3</sub> is ferromagnetic below the Curie temperature  $T_c = 14.2$  K [13,24,25] with an ordered magnetic moment of  $\sim 1.5 \mu_B/\text{Ce}$  aligned along the  $c$  axis [24]. This rather small value of the magnetic moment compared with the effective moment above  $T_c$  ( $\mu_{\text{eff}} = 2.54 \mu_B/\text{Ce}$ ) suggests some degree of delocalization of 4*f* electrons. Application of pressure suppresses the ferromagnetism, and application of magnetic field above 4.1 GPa shows a tricritical point evolving into a wing structure phase with a quantum critical point [26]. It has also been shown that the FM ordering in CeTiGe<sub>3</sub> can be linearly suppressed upon substituting Ti by V [24] and Ni [27] down to a putative FM QCP. In this study, we have induced a negative pressure by doping the Ce lattice with slightly larger La atoms to suppress the ferromagnetism of CeTiGe<sub>3</sub> and to elucidate the competing energy scales relevant to this compound. The effect of substitutions is investigated by means of electrical resistivity, magnetic susceptibility, and specific heat measurements.

**II. EXPERIMENTS**

Single crystalline samples with nominal composition,  $\text{Ce}_x\text{La}_{1-x}\text{TiGe}_3$ , were prepared by high temperature ternary melt [25]. In this report a nominal Ce-concentration  $x$ , determined by initial weight of Ce, is used. Analysis of the powder x-ray diffraction patterns shows that all samples crystallize in the hexagonal BaNiO<sub>3</sub>-type structure ( $P6_3/mmc$ ) without any trace of secondary phases. It should be noted that specific heat

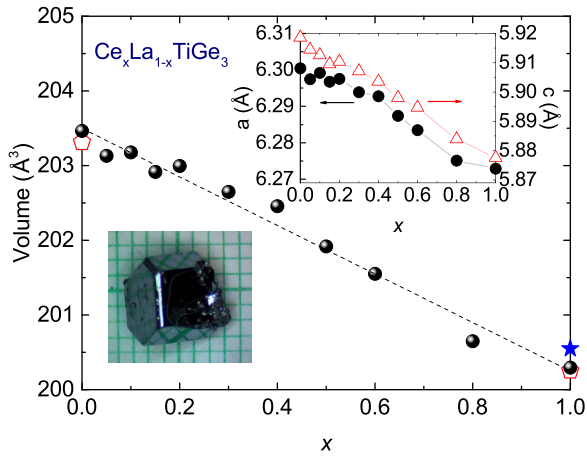


FIG. 1. Variation of unit cell volume in  $\text{Ce}_x\text{La}_{1-x}\text{TiGe}_3$ . Open symbols and star are taken from Refs. [13,24]. Top inset shows lattice parameters  $a$  (solid circles, left axis) and  $c$  (open triangles, right axis). Bottom inset shows a photograph image of  $\text{LaTiGe}_3$ .

and magnetic susceptibility measurements in earlier studies [13,24,25] indicate an anomaly around 7 K that is probably due to the presence of a ferromagnetic  $\text{CeGe}_{2-x}$  impurity phase. The Curie temperature ( $T_c = 14.2$  K) of  $\text{CeTiGe}_3$  is also confirmed by magnetic susceptibility measurements, which are in good agreement with that in previous reports [13,24,25]. For the determination of lattice parameters, the powdered samples were mixed with Si-reference powders to correct the instrumental zero shift. Figure 1 displays lattice parameters and unit cell volume as a function of Ce concentration ( $x$ ). The obtained unit cell volumes for stoichiometric  $\text{CeTiGe}_3$  and  $\text{LaTiGe}_3$  are in good agreement with reported values [13,24]. As shown in Fig. 1, the unit cell volume decreases linearly as Ce concentration increases, following the Lanthanide contraction. A volume reduction about  $\sim 1.6\%$  arises from differences in the ionic radii of  $\text{Ce}^{3+}$  and  $\text{La}^{3+}$ . It is expected that the variation of the unit cell volume and the dilution of magnetic ions in these systems will alter the competing energy scales of Kondo, RKKY, and CEF splittings as seen in other Ce- and Yb-based Kondo lattice systems.

The dc magnetization as a function of temperature from 1.8 to 300 K, and magnetic fields, up to 70 kOe, was measured in a Quantum Design (QD) Magnetic Property Measurement System (MPMS). Four-probe ac resistivity measurements were performed from 300 K down to 0.4 K in a QD Physical Property Measurement System (PPMS) with  $^3\text{He}$  option. The surfaces of the crystals were polished to remove the excess flux. Specific heat was measured by the relaxation technique down to  $T = 0.36$  K in a QD PPMS.

### III. RESULTS

#### A. $\text{LaTiGe}_3$

The temperature dependence of specific heat,  $C_p$ , of  $\text{LaTiGe}_3$  is plotted in Fig. 2(a). The  $C_p$  curves are typical of metallic compounds and do not show any signature of a phase transition. A magnetic field of 90 kOe has essentially no effect on  $C_p(T)$  as shown in Fig. 2(a). The specific heat increases rapidly between 25 and 100 K and on further warming appears

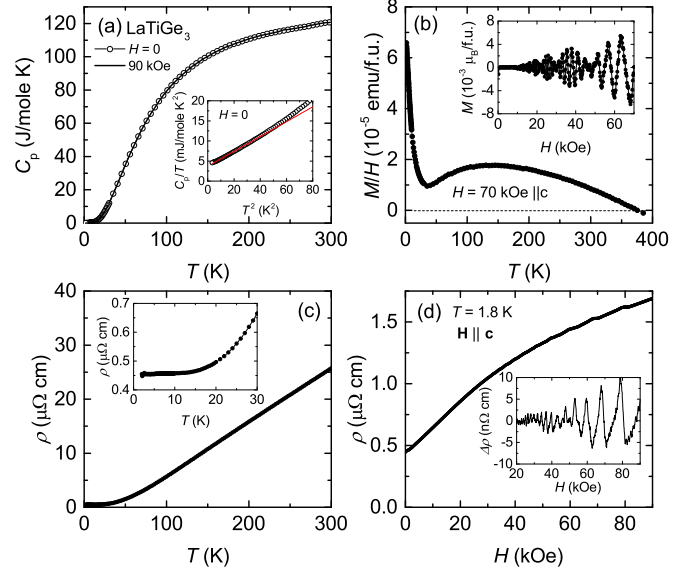


FIG. 2. Physical properties of  $\text{LaTiGe}_3$ : (a) Specific heat in  $H = 0$  (symbols) and 90 kOe (solid line) for  $H \parallel c$ . Inset displays  $C_p/T$  vs  $T^2$  plot at low temperatures. Solid line represents a linear fit. (b) Magnetic susceptibility at  $H = 70$  kOe for  $H \parallel c$ . Inset shows the magnetization as a function of field at  $T = 1.8$  K for  $H \parallel c$ . (c) Zero-field electrical resistivity. Inset shows the expanded view at low temperatures. (d) Transverse magnetoresistance at  $T = 1.8$  K. Inset shows the oscillatory component of the resistivity, subtracted background contributions using a polynomial fit.

to be saturating toward the classical limit of the Dulong-Petit law. The electronic specific heat coefficient  $\gamma$  and the Debye temperature  $\Theta_D$  of  $\text{LaTiGe}_3$  can be obtained by fitting the  $C_p$  data to the relation  $C_p = \gamma T + \beta T^3$  at low temperatures (inset). In zero field,  $\Theta_D$  is estimated to be  $\sim 200$  K and  $\gamma$  is found to be  $\sim 4$  mJ/mol  $\text{K}^2$ .

The magnetic susceptibility,  $\chi(T) = M/H$ , of  $\text{LaTiGe}_3$  depends on temperature as shown in Fig. 2(b).  $\chi(T)$  along  $H \parallel c$  shows a broad maximum at around 125 K and changes its sign from positive (paramagnetic) to negative (diamagnetic) around 375 K. There is an upward tail in  $\chi(T)$  below 30 K, which is due to the de Haas van Alphen (dHvA) effect. At low temperatures an oscillatory behavior in magnetization isotherm at  $T = 1.8$  K occurs, as shown in the inset. The oscillations are clearly detected for  $H > 8$  kOe and for temperatures as high as 50 K. This observation implies the sample used in the current study is of very high quality.

Figure 2(c) shows the temperature dependence of electrical resistivity  $\rho(T)$  curve for  $\text{LaTiGe}_3$ , where the current was applied parallel to the  $ab$  plane of hexagonal structure:  $I \parallel ab$ .  $\rho(T)$  is measured from 1.8 K to 300 K and found to be metallic; for  $50 \text{ K} < T < 300 \text{ K}$ ,  $\rho(T)$  decreases in a roughly linear fashion with decreasing temperature, below 15 K  $\rho(T)$  starts to saturate with a very small residual resistivity, and below 7 K  $\rho(T)$  is proportional to  $T^2$ . The residual resistivity ratio (RRR) determined by  $\rho(300 \text{ K})/\rho(2 \text{ K})$  is  $\sim 57$ . A power law analysis of the resistivity,  $\rho(T) = \rho_0 + AT^2$ , finds a residual resistivity  $\rho_0 = 0.45 \mu\Omega \text{ cm}$  and the coefficient  $A \simeq 4.8 \times 10^{-5} \mu\Omega \text{ cm}/\text{K}^2$ . The small value of  $A$  is consistent with the small effective mass estimated from specific heat

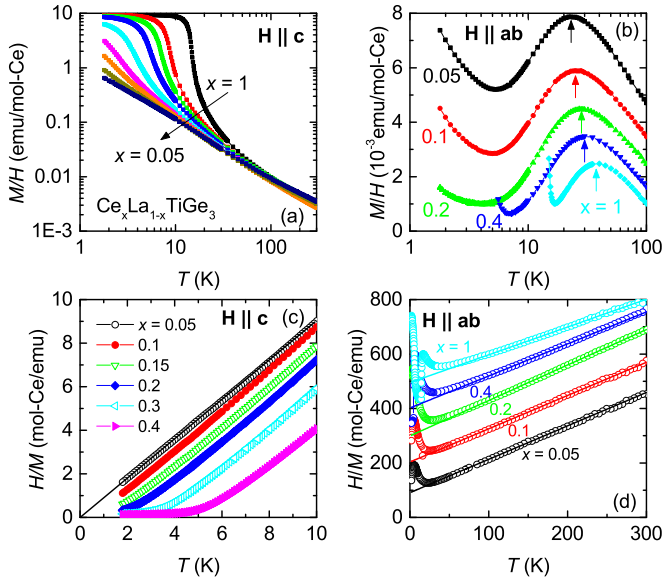


FIG. 3. (a) Temperature dependence of magnetic susceptibility ( $M/H$ ) curves for  $\text{Ce}_x\text{La}_{1-x}\text{TiGe}_3$  system, measured at  $H = 1$  kOe for  $H \parallel c$ . The curves correspond to  $x = 1, 0.8, 0.6, 0.5, 0.4, 0.3, 0.2, 0.15, 0.1, 0.05$  from top to bottom. (b)  $M/H$  for  $H \parallel ab$ . Arrows indicate the local maximum in  $\chi(T)$ . For clarity the susceptibility curves for  $x = 0.4$  and  $x = 1$  are plotted only above the  $T_c$ . (c) Inverse magnetic susceptibility ( $H/M$ ) for  $H \parallel c$  below 10 K. The solid line is a guide to the eye. (d)  $H/M$  for  $H \parallel ab$  at  $H = 1$  kOe. Solid lines represent a Curie-Weiss fit to the data. The curves are shifted vertically for clarity.

$\gamma \sim 4$  mJ/mol K<sup>2</sup>, where the Kadowaki-Wood ratio is  $A/\gamma^2 \simeq 0.3 \times 10^{-5} \mu\Omega \text{ cm (mol K/mJ)}^2$ .

Figure 2(d) shows the magnetic field dependence of the resistivity for  $H \parallel c$  at  $T = 1.8$  K. The transverse magnetoresistance is not proportional to  $H^2$  over the field range measured. There is the Shubnikov-de Haas (SdH) effect superimposed on the magnetoresistance. The amplitude of the oscillations increases with increasing magnetic field as shown in the inset. Detailed analysis of the quantum oscillations shown in both the magnetization and magnetoresistance will be published elsewhere. The low  $\rho_0$ , large RRR, and quantum oscillations indicate a very high quality of the sample.

### B. Magnetic property of $\text{Ce}_x\text{La}_{1-x}\text{TiGe}_3$

The temperature dependences of the magnetic susceptibility,  $\chi(T) = M/H$ , and the inverse magnetic susceptibility,  $1/\chi(T)$ , for both  $H \parallel ab$  and  $H \parallel c$  are shown in Fig. 3. The  $4f$ -electron component of the magnetic susceptibility is normalized to a mole of Ce. At high temperatures, the  $\chi(T)$  curves for both  $H \parallel c$  and  $H \parallel ab$  follow the Curie-Weiss law,  $\chi(T) = C/(T - \theta_p)$ , where  $C$  is the Curie constant and  $\theta_p$  is the paramagnetic Curie temperature. The fitting was performed in the temperature region between 150 K and 300 K. The effective magnetic moment,  $\mu_{\text{eff}}$ , and  $\theta_p$ , deduced from the Curie-Weiss law, as a function of  $x$  are summarized in Figs. 4(a) and 4(b), respectively. Note that  $\mu_{\text{eff}}$  and  $\theta_p$  are also estimated from the polycrystalline average;  $\chi(T) = 2/3 \chi_{ab}(T) + 1/3 \chi_c(T)$ . The obtained values

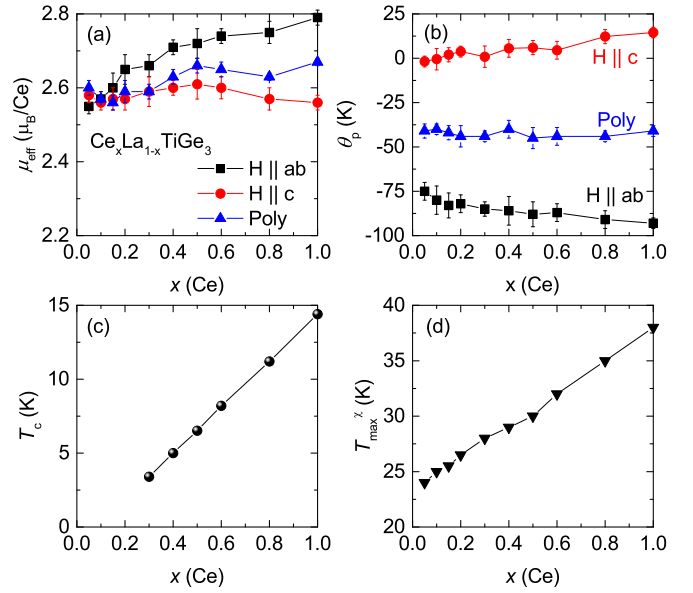


FIG. 4. (a) Effective magnetic moment  $\mu_{\text{eff}}$  as a function of  $x$  in  $\text{Ce}_x\text{La}_{1-x}\text{TiGe}_3$ . (b) Paramagnetic Curie temperature. (c) Curie temperature  $T_c$  determined from  $d\chi T/dT$  for  $H \parallel c$ . (d)  $T_{\text{max}}^{\chi}$  obtained from the maximum in  $\chi(T)$  curve for  $H \parallel ab$ .

of  $\mu_{\text{eff}}$  and  $\theta_p$  gradually vary with  $x$ . For  $x = 1$  ( $\text{CeTiGe}_3$ ),  $\mu_{\text{eff}} = 2.68 \mu_B/\text{Ce}$  for the polycrystalline average, which is somewhat higher than that of earlier studies [24,25]. The  $\mu_{\text{eff}}$  for the entire  $x$  range is close to the theoretical value ( $2.54 \mu_B$ ) of free  $\text{Ce}^{3+}$  ions. The obtained  $\mu_{\text{eff}}$  values indicate that the  $4f$  electrons in  $\text{Ce}_x\text{La}_{1-x}\text{TiGe}_3$  single crystals are well localized at high temperatures and also suggest that the electronic structures do not have a pronounced change over the entire range of  $x$ . Since the obtained  $\mu_{\text{eff}}$  indicates the  $x$  dependence, it is necessary to determine actual Ce concentration in the  $\text{Ce}_x\text{La}_{1-x}\text{TiGe}_3$  system by wavelength dispersive x-ray spectroscopy (WDS).

There is a large difference in the magnitude of  $\theta_p$  between  $H \parallel ab$  and  $H \parallel c$  as shown in Fig. 4(b). For  $\text{CeTiGe}_3$ ,  $\theta_p \sim 14$  K along the  $c$  axis,  $-93$  K in the  $ab$  plane, and  $-37.5$  K for the polycrystalline average are comparable to the earlier polycrystalline and single crystal studies [13,25]. The  $\theta_p$  for  $H \parallel ab$  is negative for the entire  $x$  range and continuously decreases as  $x$  decreases, whereas the  $\theta_p$  for  $H \parallel c$  is positive for  $x = 1$  ( $\sim 14$  K) and continuously decreases to a small negative value for  $x = 0.05$  ( $\sim -2$  K), with a sign reversal around  $x \sim 0.1$ . Although  $\text{Ce}_x\text{La}_{1-x}\text{TiGe}_3$  samples for  $x \geq 0.3$  order ferromagnetically (see below), the  $\theta_p$  values obtained from the polycrystalline average are negative and large in absolute value and weakly depend on  $x$ . This is typical for Kondo lattices (even ferromagnetic ones) since  $\theta_p$  is determined by on-site Kondo screening rather than by intersite exchange interactions. The significant anisotropic behavior of  $\theta_p$  between  $H \parallel c$  and  $H \parallel ab$  and its large negative polycrystalline average are probably due to the combined effects of the crystalline electric field (CEF) effect and the hybridization of the  $4f$  electrons with the conduction carriers.

The  $\chi_c(T)$  for  $x = 1$  shows a sharp upturn at low temperatures, as shown in Fig. 3(a), marking the long-range

ferromagnetic order, which is consistent with earlier reports [13,24,25]. The magnetic phase transition from paramagnetic (PM) to ferromagnetic (FM) is clearly observed above 1.8 K for samples with  $x \geq 0.3$ . Note that  $\chi_c(T)$  for  $x = 0.2$  starts to sharply rise below 2.5 K but does not saturate, probably due to magnetic ordering below 2 K. The phase transition temperature  $T_c$  determined by  $d\chi T/dT$  for  $H \parallel c$  is plotted in Fig. 4(c), where substituting Ce site by La ion leads to a linear reduction of  $T_c$ .

Figure 3(c) shows  $1/\chi_c(T)$  below 10 K for various values of  $x$ . Whereas  $1/\chi_c(T)$  curves for  $x = 0.05$  and  $0.1$  clearly show a linear temperature dependence ( $\chi_c(T) \propto 1/T$ ) below 10 K,  $1/\chi_c(T)$  curves for  $x \geq 0.3$  show evidence of saturating below  $T_c$ . For  $x = 0.05$ , a linear extrapolation of  $1/\chi_c(T)$  toward  $T = 0$  yields  $1/\chi_c(T \rightarrow 0) \approx 0$ . By considering the linear region in the paramagnetic state  $1/\chi_c(T \rightarrow 0)$  increases from a negative value with decreasing  $x$  and goes to zero at a concentration  $x = 0.05$ . This result suggests a possibility that the susceptibility of the dilute system exhibits a power law divergence as  $T \rightarrow 0$ . It has to be confirmed by the magnetic susceptibility measurement below 1.8 K whether this feature continues down to much lower temperatures. Note that a dilute Kondo system follows  $1/\chi(T) \propto T + T_K$  for  $T \gg T_K$  [28]. Since the magnetic susceptibility for  $x = 0.05$  and  $0.1$  follows  $\chi_c(T) \propto 1/T$  below 10 K, it is expected that the Kondo temperature of low Ce concentrations is less than 1.8 K.

The  $\chi_{ab}(T)$  curves for the entire  $x$  range show a broad local maximum at high temperatures as shown in Fig. 3(b), where the curves for  $x = 0.4$  and  $x = 1$  are plotted only above  $T_c$  for clarity. The determined maximum temperature,  $T_{\max}^{\chi}$ , is plotted in Fig. 4(d). The  $T_{\max}^{\chi} \sim 38$  K for  $x = 1$  decreases almost linearly as  $x$  decreases, reaching  $T_{\max}^{\chi} \sim 23$  K for  $x = 0.05$ . This result suggests that the CEF effect may vary linearly with  $x$ . It should be noted that the first and second excited state doublets for  $\text{CeTiGe}_3$  ( $x = 1$ ) are located at  $\sim 50$  K and  $\sim 220$  K, respectively, according to the previous inelastic neutron scattering and specific heat analysis [24,25]. Additionally it has to be noted that such a well defined maximum in  $\chi(T)$  is a typical feature of Kondo lattice systems with a large ground state degeneracy as discussed in Ref. [29]. However, the maximum in  $\chi_{ab}(T)$  curves cannot be solely fitted by the Kondo contribution and the resulting ground state degeneracy is not consistent with the specific heat analysis (see below).

Figure 5(a) shows the isothermal magnetization curves,  $M(H)$ , for  $\text{Ce}_x\text{La}_{1-x}\text{TiGe}_3$  single crystals, measured at  $T = 1.8$  K up to  $H = 70$  kOe along the  $c$  axis. For  $x = 1$ , the magnetization curve shows a saturation tendency above the critical field  $H_c \sim 1.3$  kOe, denoted by the arrow in Fig. 5(b), and the magnetization value at  $H = 70$  kOe is in good agreement with the earlier neutron data for polycrystalline sample [24] and magnetization measurement for the single crystal [25]. The  $M(H)$  curves tend to be saturated rapidly at low fields for  $x \geq 0.3$  samples, whereas  $M(H)$  curves for  $x < 0.3$  show the Brillouin functionlike behavior. Hysteresis is clearly observed below  $H_c$  for  $x \geq 0.3$  samples as shown in Fig. 5(b), corroborating the ferromagnetic nature of the magnetic transition.

A relatively large anisotropy in the magnetization is observed, with the response  $M_c(H)$  for  $H \parallel c$  being

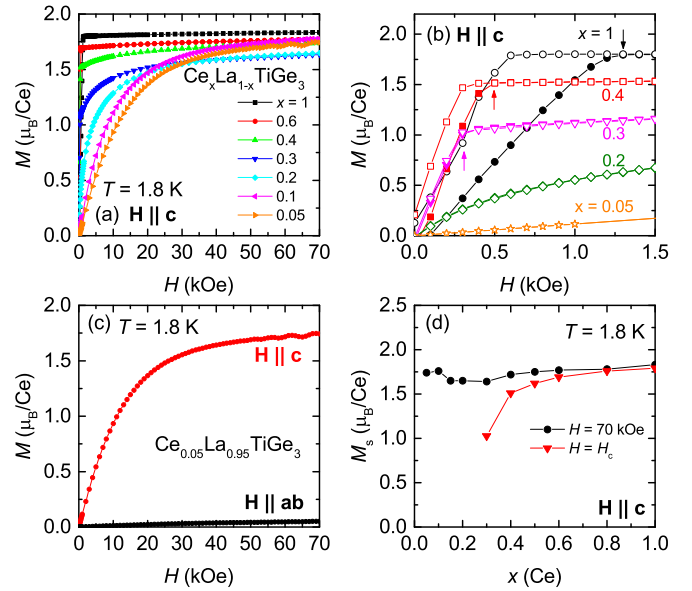


FIG. 5. (a) Magnetic field dependences of magnetization  $M(H)$  curves for  $H \parallel c$  at  $T = 1.8$  K. (b) Extended plot in the low field region of  $M(H)$  curves for  $H \parallel c$ . Solid symbols and open symbols are up- and down-sweep of magnetic fields, respectively. Arrows indicate the critical fields. (c)  $M(H)$  curves of  $\text{Ce}_{0.05}\text{La}_{0.95}\text{TiGe}_3$  at  $T = 1.8$  K for both  $H \parallel ab$  and  $H \parallel c$ . (d) Magnetization values for  $H \parallel c$  at  $T = 1.8$  K as a function of  $x$ . Solid circle and triangular symbols are taken at  $H = 70$  kOe and at the critical fields, respectively.

substantially larger than  $M_{ab}(H)$  for  $H \parallel ab$  at low temperatures. The large value of the magnetization for  $H \parallel c$  direction establishes the  $c$  axis as the easy magnetization direction. It should be noted that for  $H \parallel ab$  we were not able to reliably measure the magnetization below  $T_c$  due to the strong torque. Thus,  $M_{ab}(H)$  curves for  $x > 0.1$  are not shown here. For  $x = 0.05$ , as a representative example,  $M(H)$  curves for both  $H \parallel c$  and  $H \parallel ab$  are plotted in Fig. 5(c). The  $M_c(H)$  curve clearly shows dHvA oscillations for  $H > 50$  kOe, indicating relatively high quality of sample.

Figure 5(d) displays the magnetization values at  $T = 1.8$  K and  $H = 70$  kOe along the  $c$  axis. It is clear that the  $M(H)$  value for various  $x$  depends weakly on  $x$ , where the magnetization reflects both ferromagnetic and paramagnetic contributions. The effective moment of Ce, obtained from Curie-Weiss fit for  $T \gg T_c$ , is almost independent of  $x$  [Fig. 4(a)] and corresponds to  $J = 5/2$ . The value of magnetization at 70 kOe is somewhat smaller than the theoretical value  $gJ = 2.14 \mu_B$  for the  $J = 5/2$  free ion value of  $\text{Ce}^{3+}$ . For  $x \geq 0.3$ , the magnetization value at the critical field is also plotted in Fig. 5(d) as a function of  $x$ . As can be seen from the plot, the magnetization value increases as  $x$  increases. Note that because the measurement temperature of 1.8 K for low  $x$  region is quite close to the  $T_c$ , the thermal effects cannot be safely neglected.

### C. Specific heat of $\text{Ce}_x\text{La}_{1-x}\text{TiGe}_3$

The temperature dependence of specific heat,  $C_p(T)$ , per formula unit of  $\text{Ce}_x\text{La}_{1-x}\text{TiGe}_3$  is shown in Fig. 6. At 300 K,

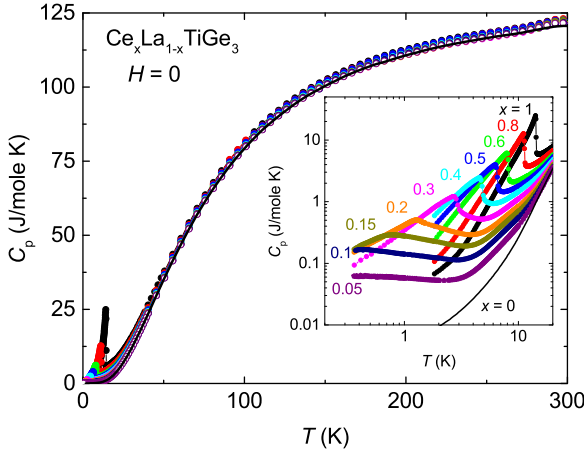


FIG. 6. Specific heat curves for  $\text{Ce}_x\text{La}_{1-x}\text{TiGe}_3$ . Inset shows the expanded plot below 20 K in log-log scale.

all  $C_p(T)$  curves reach  $\sim 125$  J/mole K, which is close to the Dulong-Petit limit. Above 100 K, the temperature variation of the specific heat for  $0.05 \leq x \leq 1$  are similar to the nonmagnetic analogue  $\text{LaTiGe}_3$ . For  $x = 1$ , the specific heat curve is consistent with earlier reports [13,24,25] however indicates no impurity contribution in our measurement. Note that a minor anomaly near  $7 \sim 8$  K in specific heat has been observed for the polycrystalline  $\text{CeTiGe}_3$  [13] and  $\text{CeTi}_{0.75}\text{V}_{0.25}\text{Ge}_3$  [24] samples due to the  $\text{CeGe}_{2-x}$  ferromagnetic impurity phase [30–32]. In addition, the anomaly in magnetic susceptibility along the  $a$  axis has also been detected for the single crystal sample [25]. In this study, however, the contribution of the minor impurity phase of  $\text{CeGe}_{2-x}$  has not been detected for any  $\text{Ce}_x\text{La}_{1-x}\text{TiGe}_3$  samples. At low temperatures, a clear  $\lambda$ -like peak for  $x \geq 0.3$  and somewhat broadened  $\lambda$ -shape anomaly for  $0.15 \leq x < 0.3$  in  $C_p(T)$  curves reflect the FM transition as shown in the inset of Fig. 6. The peak position corresponding to each  $x$  is plotted in Fig. 7(d), where a linear reduction of  $T_c$  with decreasing  $x$  can be clearly seen.

To obtain the magnetic part of the specific heat,  $C_m$ , for  $x \geq 0.05$  the electronic and phonon contributions to the specific heat of  $\text{LaTiGe}_3$  and subtracted from the data. Figure 7(a) shows the magnetic part of the specific heat curves,  $C_m = C_p(\text{Ce}_x\text{La}_{1-x}\text{TiGe}_3) - C_p(\text{LaTiGe}_3)$ , normalized to a mole of Ce. The  $C_m$  for  $x = 1$  indicates a broad local maximum (electronic Schottky-like maximum) around  $T_{\text{max}}^{C_m} \sim 20$  K just above  $T_c$ . In the previous study, the analysis of  $C_m$  for  $\text{CeTiGe}_3$  has suggested that the broad feature is mainly due to the relatively low lying first excited CEF doublet located at  $\sim 50$  K [25]. With La substitution, the broad maximum is clearly discernible and moves towards lower temperatures accompanied by a reduction in maximum value. The position of the broad maximum  $T_{\text{max}}^{C_m}$  is plotted in Fig. 7(d). For  $x = 0.05$  and  $0.1$ , a clear maximum occurs at about 13 K and a broad feature develops at lower temperatures, which can be associated with the CEF effect and Kondo screening.

Figure 7(b) presents the temperature dependence of  $C_m/T$  curves (normalized to a mole of Ce) for various values of  $x$ , which also clarify the ordered state and underlying electronic behavior. It can be clearly seen that the  $T_c$  moves to lower

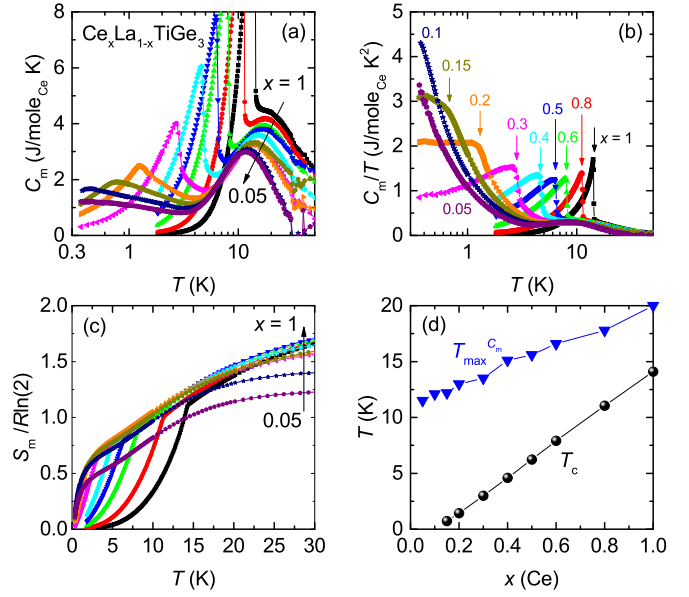


FIG. 7. (a) Magnetic part of specific heat  $C_m$  curves for  $\text{Ce}_x\text{La}_{1-x}\text{TiGe}_3$ , where  $x = 1, 0.8, 0.6, 0.5, 0.4, 0.3, 0.2, 0.15, 0.1$ , and  $0.05$  from top to bottom. (b)  $C_m/T$  curves. Vertical arrows indicate the peak position in  $C_m$ . (c) Magnetic entropy  $S_m$  curves. (d) The broad local maximum  $T_{\text{max}}^{C_m}$  and the phase transition temperature  $T_c$  as a function of  $x$ .

temperatures with decreasing  $x$ . The arrows in the figure indicate the peak position developed in  $C_m$ . For  $x \leq 0.2$ , the feature corresponding to the FM transition broadens and is superimposed on an increasing additional electronic contribution. The broadening of the phase transition is probably related to the variation on the atomic scale of the Ce and La concentration. A dramatic increase of the low temperature  $C_m/T$  curve is observed for  $x \leq 0.3$ , where  $C_m/T \approx 0.8$  J/mol  $\text{K}^2$  at  $T = 0.4$  K for  $x = 0.3$  and  $C_m/T \approx 4.3$  J/mol  $\text{K}^2$  for  $x = 0.1$ . This enormous change of the  $C_m/T$  values at lowest temperatures corroborates with a rough estimation of the growth of the Kondo contribution with decreasing  $x$  in  $\text{Ce}_x\text{La}_{1-x}\text{TiGe}_3$  ( $T_K \propto 1/\gamma$  [33]). As  $T_c$  approaches zero near  $x_c \sim 0.1$ , the  $C_m/T$  curve does not show a conventional saturation behavior toward  $T \rightarrow 0$ ; instead, it shows a divergent behavior down to the lowest measured temperature. Interestingly, the  $C_m/T$  for  $x = 0.05$  indicates a power law divergence ( $C_m/T \propto 1/T$ ), which is stronger than the logarithmic divergence.

The magnetic entropy  $S_m$  curves for all samples are plotted in Fig. 7(c). Since the  $C_m/T$  curves for  $x = 0.05$  and  $0.1$  continuously increase as the temperature decreases, the extrapolation of the specific heat to  $T = 0$  cannot be made without any ambiguities. Thus, the entropy is estimated by integrating the  $C_m/T$  curve from the base temperature of the present experiment. This will clearly underestimate the total magnetic entropy, especially at low temperatures. It can be seen that  $S_m$  for  $x = 1$  reaches a larger value than  $R \ln(2)$  at  $T_c$ , indicating that the CEF splitting is small so that the entropy associated with the higher CEF levels contributes [25]. Above  $T_c$ , the entropy continues to rise due to the contribution of the excited state CEF levels. By considering  $S_m$ , it can be inferred that the FM order is associated with the doublet ground state

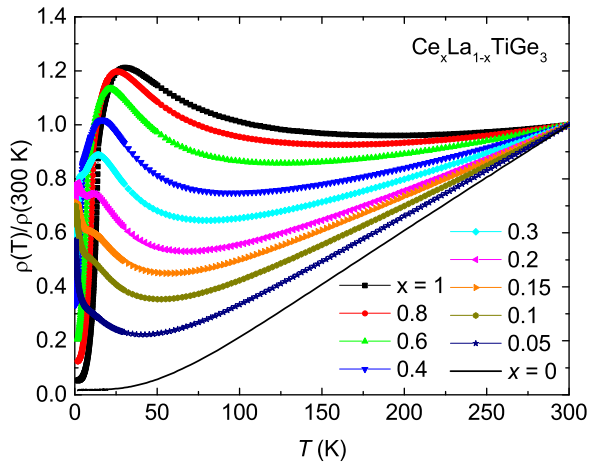


FIG. 8. Electrical resistivity  $\rho(T)$  curves, normalized to 300 K, for  $\text{Ce}_x\text{La}_{1-x}\text{TiGe}_3$ .

as expected from the CEF effect on the Kramers Ce ion in hexagonal symmetry. In the  $x$  region where the phase transition remains sharp ( $0.3 < x \leq 1$ ),  $S_m$  at  $T_c$  is continuously decreasing with decreasing  $x$ , suggesting that the strength of the hybridization changes over this range. For samples with smaller concentrations that still show ferromagnetism but have broadened phase transitions ( $0.1 < x < 0.3$ ), the entropy recovered at  $T_c$  reduces further with decreasing  $x$ , which indicates strengthening hybridization. Above  $T_c$ , all entropy curves for  $x > 0.15$  merge into a single curve, whereas the entropy curves for  $x = 0.05$  and  $x = 0.1$  are smaller than other concentrations. It is expected that, when the missing entropy below the measured base temperature (below 0.36 K) is considered, the entropy curves for  $x = 0.05$  and  $0.1$  will merge into the single curve like other concentrations.

#### D. Electrical resistivity of $\text{Ce}_x\text{La}_{1-x}\text{TiGe}_3$

Figure 8 shows the temperature dependence of electrical resistivity,  $\rho(T)$ , for  $\text{Ce}_x\text{La}_{1-x}\text{TiGe}_3$  for currents in the  $ab$  plane, where the curves are normalized to 300 K:  $\rho(T)/\rho(300 \text{ K})$ . For  $x = 0$  ( $\text{LaTiGe}_3$ ), the resistivity curve exhibits ordinary metallic behavior with a small residual resistivity of  $\sim 0.45 \mu\Omega \text{ cm}$ . For  $x = 1$  ( $\text{CeTiGe}_3$ ), typical Kondo lattice behavior is confirmed by a minimum, followed by logarithmic increase and a well pronounced maximum at around 30 K, which is consistent with the earlier single crystal study [25]. Below 14.5 K the resistivity drastically decreases, saturating at the residual resistivity of  $\rho_0 \sim 6 \mu\Omega \text{ cm}$ . Such a pronounced decrease is typical for the formation of a magnetic ordering, losing the spin disorder scattering. For  $0 < x \leq 1$ , as the temperature is decreased from 300 K,  $\rho(T)$  curves decrease monotonically and reach a minimum, followed by a logarithmic increase. At low temperatures, the  $\rho(T)$  curves for  $x \geq 0.15$  clearly indicate an abrupt resistivity drop below  $T_c$ , as indicated by arrows in Fig. 9(a), reducing the electron scattering due to the removal of spin disorder scattering. The  $T_c$  is determined from the peak position in  $d\rho(T)/dT$  analysis and plotted in Fig. 9(d). As can be seen from the figure,  $T_c$  decreases linearly as  $x$  decreases. For small  $x$  the phase transition broadens, probably due to the disorder, and

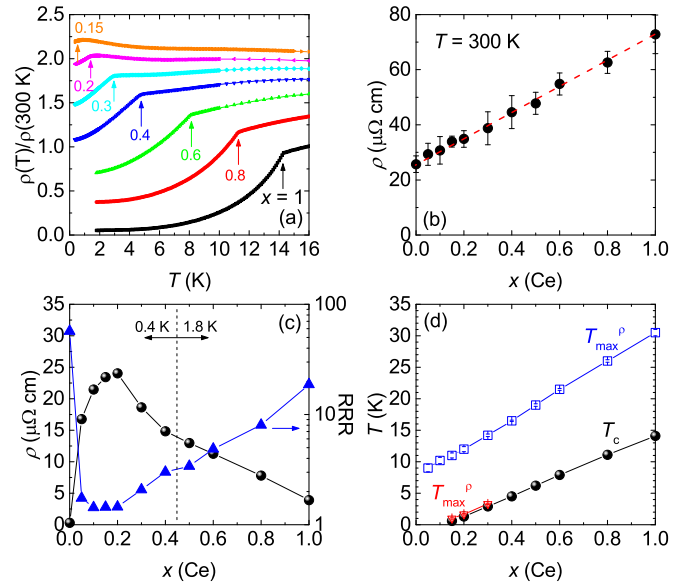


FIG. 9. (a)  $\rho(T)$  curves for  $\text{Ce}_x\text{La}_{1-x}\text{TiGe}_3$  below 16 K. Arrows indicate the peak position in  $d\rho(T)/dT$ . (b) Resistivity value at 300 K as a function of  $x$ . Error bars represent the geometry (dimensional) error. Dashed line is a guide to the eye. (c) Resistivity value at 0.4 K for  $x \leq 0.4$  and at 1.8 K for  $x > 0.5$  (left axis) and residual resistivity ratio RRR (right axis) as a function of  $x$ . (d) Local maximum  $T_{\max}^{\rho}$  and  $T_c$  as a function of  $x$ . See details in text.

continues to be suppressed until it is no longer visible near  $x = 0.1$ .

For  $\text{Ce}_x\text{La}_{1-x}\text{TiGe}_3$  systems, the absolute value of the resistivity at 300 K continuously increases as  $x$  increases, as shown in Fig. 9(b), implying that the magnetic Kondo scattering increases with increasing Ce concentration. In other words, the resistivity at 300 K increases as volume decreases, which is consistent with earlier pressure dependence of resistivity measurements [26]. At 300 K the electrical resistivity of  $\text{CeTiGe}_3$  under external pressure increases linearly with a rate of  $7.4 \mu\Omega \text{ cm/GPa}$  up to 5.76 GPa [26]. For  $x = 1$ , the residual resistivity ratio,  $\text{RRR} = \rho(300 \text{ K})/\rho(1.8 \text{ K})$  is  $\sim 20$ , which is comparable to the earlier single crystal studies [25,26]. The obtained RRR for entire  $x$  ranges, determined by  $\rho(300 \text{ K})/\rho(1.8 \text{ K})$  for  $x \geq 0.5$  and  $\rho(300 \text{ K})/\rho(0.4 \text{ K})$  for  $x \leq 0.4$ , is plotted in Fig. 9(c). The resistivity value at the base temperature measured is also plotted in Fig. 9(c), where it can be approximated to be the residual resistivity. The RRR decreases with decreasing  $x$  for  $0.3 \leq x \leq 1$  and becomes small in the dilute limit ( $0.05 \leq x \leq 0.2$ ). The La-substituted samples do not simply follow a Nordheim's like contribution,  $\rho(T = 0) \propto x(1 - x)$ , to the residual resistivity, where a maximum residual resistivity is shown around  $x = 0.2$ . Since both RRR and residual resistivity deviate from the Nordheim's rule, it has to be considered the combination of disorder effect and scattering with Ce moment to explain the evolution of resistivity curves for  $\text{Ce}_x\text{La}_{1-x}\text{TiGe}_3$  system.

To elucidate the magnetic Kondo scattering, the magnetic contribution to the resistivity  $\rho_m$  for  $x > 0$  is estimated by the difference between the resistivities of  $\text{Ce}_x\text{La}_{1-x}\text{TiGe}_3$  and  $\text{LaTiGe}_3$ :  $\rho_m = \rho(\text{Ce}_x\text{La}_{1-x}\text{TiGe}_3) - \rho(\text{LaTiGe}_3)$ . The

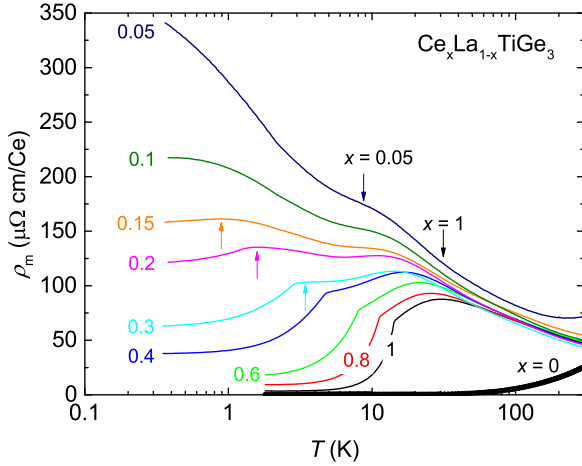


FIG. 10. The magnetic contribution to the resistivity  $\rho_m$  for  $x > 0$ , where  $x = 0$  curve is plotted together for comparison. Down arrows indicate a local maximum developed at high temperatures and up arrows indicate the position of a local maximum in the low temperature side.

resulting  $\rho_m$  per at % Ce is plotted in Fig. 10, providing compelling evidence for scaling behavior with the Ce concentration. We note that  $\rho_m$  for  $x = 0.05$  does not collapse onto the single curve at high temperatures. This deviation from the scaling behavior is probably due to the sample geometry error. The  $-\log(T)$  dependence of the  $\rho_m$  curves for all  $x$  strongly suggests that the resistivity of  $\text{Ce}_x\text{La}_{1-x}\text{TiGe}_3$  system is governed by the Kondo effect and the high temperature Kondo contribution is essentially independent of Ce concentration. Note that as the temperature is raised above 200 K, a small increase in  $\rho_m$  [deviating from  $-\log(T)$  dependence] is observed, implying contributions of the excited state CEF levels. In the Ce-rich region, each  $\rho_m$  clearly reveals a broad maximum that generally defines the coherence temperature in a Kondo lattice system, where the coherence temperature systematically decreases with decreasing Ce concentration. In the La-rich region,  $\rho_m$  for  $x = 0.1$  shows the single ion behavior with a saturation of resistivity at low temperatures. For  $x = 0.05$ ,  $\rho_m$  indicates a tendency of saturation with decreasing temperature below 1 K. The Kondo lattice and single ion regimes are separated roughly around  $x = 0.1$ . It would be interesting to compare the critical concentration, changing the behavior from single-ion to Kondo lattice, to the percolation limit of the hexagonal lattice system. The  $\rho_m$  values at the measured base temperature continuously increase with decreasing  $x$ .

At high temperatures the resistivity curves of all Ce-containing samples reveal a broad local maximum  $T_{\max}^{\rho}$  (Figs. 8 and 10), where  $T_{\max}^{\rho}$  linearly decreases from  $\sim 32$  K ( $x = 1$ ) to  $\sim 8$  K ( $x = 0.05$ ) with decreasing Ce concentration as shown in Fig. 9(d). At low temperatures the resistivity curves for  $x < 0.4$  develop additional features below the  $T_{\max}^{\rho}$ . As clearly seen from Fig. 10, with decreasing temperature, the resistivity curves increase quasilinearly in narrow temperature regimes and either form an additional maximum just above  $T_c$  as seen for  $x = 0.3, 0.2,$  and  $0.15$  (vertical arrows in Fig. 9) or saturate at low temperatures as seen for

$x = 0.1$ . Note that the resistivity measurement below 0.4 K for  $x = 0.1$  and  $0.05$  is necessary to confirm whether the resistivity saturates (single ion behavior) or actually forms a local maximum (coherence effect in Kondo lattice). The observed maxima shown in both high temperature ( $0 < x \leq 1$ ) and low temperature ( $0.15 \leq x \leq 0.3$ ) are plotted in Fig. 9(d), where both maxima are labeled as  $T_{\max}^{\rho}$ . Note that for low  $x$  regimes, we extract the maxima assuming the curves consist of two peaks.

In general, the maxima developed in  $\rho(T)$  can be related to the Kondo effect acting on the CEF multiplets. If the Kondo temperature  $T_K$  is defined as the maximum temperature of the  $\rho(T)$  vs  $\log(T)$  curve, in a similar way to a Kondo lattice system,  $T_K$  decreases monotonically from 32 K for  $x = 1$  to about 8 K for  $x = 0.05$ . However, the single ion behavior and two local maxima for the low- $x$  regime cannot be explained by this definition. Therefore, it is natural to assume that the low temperature maximum and saturation behavior can be related to the Kondo effect acting on the ground state doublet, while the high temperature maximum can be associated with a first excited state doublet. For  $x \geq 0.5$ , the presence of a single local maximum is probably due to the comparable energy scales of  $T_K$  and the CEF energy level splitting  $\Delta_{\text{CEF}}$  between ground and first excited state doublet:  $T_K \sim \Delta_{\text{CEF}}$ . Note that the pressure dependence of resistivity measurement for  $\text{CeTiGe}_3$  clearly indicates that the  $T_{\max}^{\rho} \sim 31$  K at ambient pressure exponentially increases as the pressure increases, where the  $T_{\max}^{\rho}$  reaches  $\sim 82$  K at 5.76 GPa [26]. In other words, the lattice expansion (negative pressure) causes the decrease of the high temperature maximum  $T_{\max}^{\rho}$  in resistivity.

#### IV. DISCUSSIONS

The  $x$ - $T$  phase diagram of  $\text{Ce}_x\text{La}_{1-x}\text{TiGe}_3$ , obtained from the measurements of the magnetic susceptibility Fig. 4(c), specific heat Fig. 7(d), and electrical resistivity Fig. 9(d), is presented in Fig. 11(a). Although the  $T_c$  determined from  $d\chi T/dT$  is somewhat higher than that from  $C_p(T)$  and  $d\rho(T)/dT$ , the  $x$  dependence of the FM ordering temperature  $T_c$  is consistent for all measurements. At first glance,  $\text{Ce}_x\text{La}_{1-x}\text{TiGe}_3$  features a simple phase diagram, where the  $T_c$  is linearly suppressed with decreasing  $x$  and vanishes around the critical concentration  $x_c \sim 0.1$ . For  $x > 0.2$ , the phase transition remains relatively sharp, however for  $x \leq 0.2$  the phase transition broadens as shown in Fig. 11(b) for  $x = 0.15$ . The  $d\rho(T)/dT$  clearly indicates a slope change at  $T_c \sim 0.72$  K, while the  $C_m(T)$  shows a maximum at  $\sim 0.74$  K. Since no sudden jump in the  $C_m(T)$  curve is observed, the  $T_c$  is determined from the maximum temperature in  $C_m$ . For both  $x = 0.05$  and  $0.1$ , the phase transition should be checked by measurements below 0.4 K to confirm whether the  $T_c$  is linearly suppressed or has a tail. It should be noted that the FM transition for  $x \geq 0.3$  is clearly confirmed from the magnetization measurements. However, the nature of the (ferromagnetic) transition for  $0.15 \leq x < 0.3$  must be confirmed by measuring the magnetization below 1.8 K. In this  $x$  range resistivity and specific heat measurements indicate no thermal hysteresis below  $T_c$  within the resolution of the measurements.

The magnetic ordering in the  $\text{Ce}_x\text{La}_{1-x}\text{TiGe}_3$  system survives for a small amount of Ce, where only  $\sim 15\%$  Ce

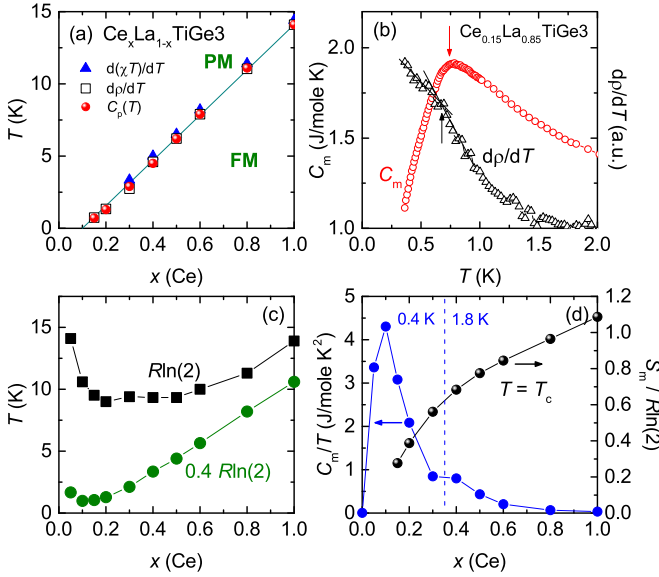


FIG. 11. (a)  $x$ - $T$  phase diagram for  $\text{Ce}_x\text{La}_{1-x}\text{TiGe}_3$ . The symbols are obtained from  $d\rho(T)/dT$ ,  $d\chi T/dT$ , and the maximum in  $C_p(T)$ . Dotted line is a guide to the eye. (b)  $C_m$  and  $d\rho(T)/dT$  for  $x = 0.15$ . Arrows indicate the determined phase transition temperature. (c) Onset temperatures reaching  $R\ln(2)$  and  $0.4R\ln(2)$  magnetic entropy. (d)  $C_m/T$  at  $T = 0.4$  K for  $x < 0.4$  and at  $1.8$  K for  $x \geq 0.4$  (left axis) and magnetic entropy  $S_m/R\ln(2)$  at  $T_c$  (right axis).

substitution into nonmagnetic  $\text{LaTiGe}_3$  background induces the magnetic order at  $\sim 0.72$  K. Note that substituting Ti with V and Ni leads to a linear decrease of  $T_c$  which disappears at the critical concentration  $x_c \sim 0.4$  for both  $\text{CeTi}_{1-x}\text{V}_x\text{Ge}_3$  and  $\text{CeTi}_{1-x}\text{Ni}_x\text{Ge}_3$  systems [24,27]. For the  $\text{Ce}_x\text{La}_{1-x}\text{TiGe}_3$  system the  $T_c$  is linearly suppressed as the unit cell volume increases, whereas for  $\text{CeTi}_{1-x}\text{V}_x\text{Ge}_3$  and  $\text{CeTi}_{1-x}\text{Ni}_x\text{Ge}_3$  systems the  $T_c$  is linearly suppressed as the unit cell volume decreases [24,27]. It has been shown that  $T_c$  of  $\text{CeTiGe}_3$  increases to higher temperatures under hydrostatic pressure up to 10 kbar and then continuously decreases up to  $\sim 40$  kbar [26]. It is expected that the increasing  $3d$ -electron density introduced by substituting V and Ni for Ti leads to an increase of the density of states at the Fermi level and also the Kondo coupling, thus suppressing the FM order. Since the ion radius of  $\text{La}^{3+}$  is larger than that of  $\text{Ce}^{3+}$ , an increase in La concentration corresponds to the increase in the unit cell volume. This may result in reduced hybridization between  $4f$  and conduction electrons.

At high temperatures, the thermodynamic and transport properties of  $\text{Ce}_x\text{La}_{1-x}\text{TiGe}_3$  can be understood qualitatively by considering the multiple energy scales of Kondo ( $T_K$ ) and RKKY ( $T_c$ ) interactions as well as the CEF effect ( $T_{\max}$ ). In Fig. 12, the maximum temperatures observed in  $\chi(T)$  along  $H \parallel ab$ ,  $C_m(T)$ , and  $\rho(T)$  data and the Weiss temperatures along  $H \parallel ab$  ( $\theta_p^{ab}$ ) and  $H \parallel c$  ( $\theta_p^c$ ) are plotted as a function of  $x$ , where the  $T_{\max}^X$  and  $\theta_p^{ab}$  are rescaled as  $T_{\max}^X/2$  and  $\theta_p^{ab}/6$ , respectively. The variation of  $T_{\max}^X$  follows the same trend as  $T_{\max}^{C_m}$  with  $T_{\max}^X = 2 \times T_{\max}^{C_m}$  for the entire  $x$  range. The variation of the high temperature  $T_{\max}^\rho$  follows a similar

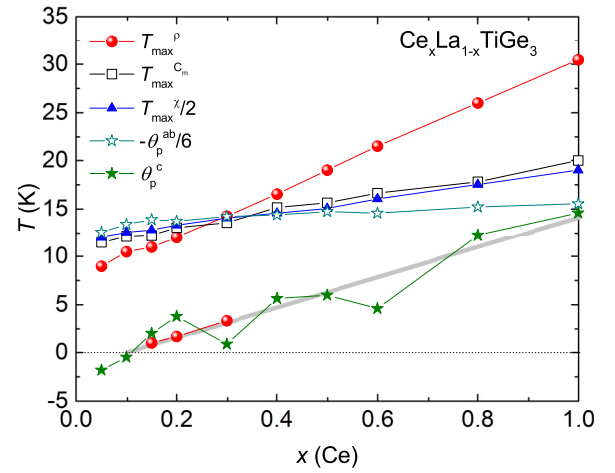


FIG. 12. Local maximum temperatures developed in the magnetic susceptibility, specific heat, and electrical resistivity and the Weiss temperatures  $\theta_p$  along  $H \parallel ab$  and  $H \parallel c$ . The solid line indicates a phase boundary between PM and FM, presented in Fig. 11(a).

trend as  $T_{\max}^X/2$  and  $T_{\max}^{C_m}$  but with different slope. It should be noted that  $\rho(T)$  curves show two local maxima for  $x = 0.15$ ,  $0.2$ , and  $0.3$ , whereas  $\chi(T)$  and  $C_m(T)$  curves show only a clear local maximum at high temperatures. At high Ce concentrations, the sharp peaks in  $C_m(T)$  due to magnetic ordering ride on top of broader peaks due to the Kondo effect, where the Kondo contribution is difficult to discern from the magnetic ordering. It is clear from resistivity measurements that there should be some Kondo screening of the  $f$  moments by the conduction electrons. Since the  $\rho(T)$  curves for small  $x$  clearly indicate a single ion behavior below the high temperature maximum, the  $\text{Ce}_x\text{La}_{1-x}\text{TiGe}_3$  system changes from the Kondo lattice for  $x = 1$  to a single ion for  $x = 0.05$  as  $x$  decreases. The observed behaviors can be attributed to the interplay between Kondo and CEF effects.

Based on the earlier specific heat analysis, the  $J = 5/2$  ground state of  $\text{CeTiGe}_3$  splits into three doublets under the action of the CEF, locating the first excited state  $\Delta_{E1} \sim 50$  K and second excited state  $\Delta_{E2} \sim 220$  K [25], which is consistent with the current specific heat results. In the discussion below, the higher excited state energy level will be ignored, considering only the size of the CEF level splitting  $\Delta_{\text{CEF}}$  between the ground state doublet and first excited doublet energy level. In a Kondo lattice system, a single maximum in  $C_m(T)$  is expected when  $T_K$  is either close to or higher than  $\Delta_{\text{CEF}}$ . When  $T_K$  is smaller than  $\Delta_{\text{CEF}}$  more than one broad local maximum has been frequently observed in the thermodynamic and transport measurements [28,34–37]. The low temperature maximum is usually located close to  $T_K$ , and the high temperature maximum is attributed to Kondo scattering off of the thermally populated CEF levels [28,37]. Thus, the local maxima developed in specific heat and resistivity can be represented as  $T_K$  and  $\Delta_{\text{CEF}}$  as relevant energy scales in Kondo lattice systems.

For  $x = 1$ , the  $C_m$  data above  $T_c$  cannot be explained solely by the Kondo contribution, with a reasonable value of  $T_K$  under the constraint of entropy balance, unless the electronic Schottky contribution due to  $\Delta_{\text{CEF}}$  is taken into account. Thus,



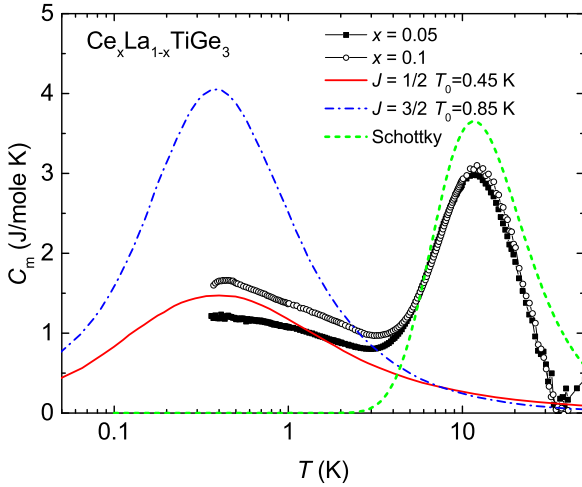


FIG. 13.  $C_m$  curves for  $x = 0.05$  and  $0.1$ . The solid and dash-dotted line represent the  $J = 1/2$  C-S model with  $T_0 = 0.45$  K and  $J = 3/2$  C-S model with  $T_0 = 0.85$  K, respectively [29]. The dotted line is based on the two level Schottky contribution with  $\Delta_{\text{CEF}} \sim 28$  K.

a single broad maximum above  $T_c$  in  $C_m$  is reflecting the combined action of Kondo and CEF effects due to the relatively small CEF level splitting ( $T_K \sim \Delta_{\text{CEF}}$ ). Note that it has been suggested in Ref. [24] that  $\Delta_{\text{CEF}}/T_K = 2$  for  $\text{CeTiGe}_3$  based on Ref. [38]. However, the temperature dependence and magnitude of  $C_m$  curve in this study is better described by the  $\Delta_{\text{CEF}}/T_K = 0$  or  $\Delta_{\text{CEF}}/T_K = 1$  case in Ref. [38]. For the dilute limit of  $x = 0.05$  and  $0.1$ , it is expected that the broad feature below 2 K and the Schottky-like maximum around 12 K in the  $C_m$  curves are associated with Kondo effects on the ground state doublet and thermally populated CEF levels, respectively ( $T_K < \Delta_{\text{CEF}}$ ). In this  $x$  range, based on the ground state degeneracy inferred from the entropy, the  $T_K$  and  $\Delta_{\text{CEF}}$  can be estimated from the analysis of the  $C_m$  data by considering both the Coqblin-Schrieffer (C-S) model [29] and electronic Schottky contributions. A fit to the  $C_m$  curves over a wide temperature range is shown in Fig. 13. Although the absolute values of  $C_m$  cannot be reliably reproduced by the fit, the temperature dependence of  $C_m$  curves can be qualitatively described by the  $J = 1/2$  C-S model with  $T_0 \sim 0.45$  K for the low temperature broad feature and the electronic Schottky contribution with  $\Delta_{\text{CEF}} \sim 28$  K for the high temperature maximum. In Fig. 13, the curve for the  $J = 3/2$  C-S model is plotted together for comparison [29]. This analysis qualitatively suggests that the high temperature maximum is being associated with the CEF effect and the low temperature broad feature with highly enhanced electronic specific heat coefficient is due to Kondo screening of the  $f$  electrons. This analysis is consistent with the entropy evolution, where the magnetic entropy continuously rises toward  $R \ln(4)$  at 30 K as shown in Fig. 7(c). Thus, in the dilute limit of  $x$ , the Kondo energy scale is clearly smaller than the energy scale of the  $\Delta_{\text{CEF}}$ . As  $x$  increases, the variation of the maximum height and maximum temperature observed in  $C_m$  curves (Fig. 7) can be correlated with a crossover from  $T_K < \Delta_{\text{CEF}}$  for  $x = 0.05$  to  $T_K \approx \Delta_{\text{CEF}}$  for  $x = 1$ . This analysis is also consistent with the behavior observed in resistivity

measurements, whereas for low  $x$  the single ion behavior is related to the Kondo scattering on the ground state doublet, for high  $x$  the local maximum  $T_{\text{max}}^\rho$  is obviously due to the Kondo screening of both the ground state and first excited state doublet. In addition, this analysis suggests that the  $T_K$  decreases more strongly than the  $\Delta_{\text{CEF}}$  when  $x$  decreases. It should be noted that for the intermediate  $x$  regimes, the separation of energy scales cannot be reliably performed, where details of the underlying Kondo effect are masked by the FM ordering and CEF splitting.

In order to better understand the competing energy scales in the  $\text{Ce}_x\text{La}_{1-x}\text{TiGe}_3$  system, the onset temperature where the magnetic entropy  $S_m$  reaches the  $R \ln(2)$  limit is plotted in Fig. 11(c) and the entropy  $S_m(T = T_c)$  released at  $T_c$  for  $x \geq 0.15$  is plotted in Fig. 11(d) as a function of  $x$ . Note that the missing entropy below the measured base temperature must be considered, especially for low- $x$  regimes. For the heavy fermion system with a ground state doublet undergoing magnetic order, the  $R \ln(2)$  entropy is recovered only at  $T \gg T_K$  [28]. As  $x$  increases, the rise of the onset temperature reaching  $R \ln(2)$  signals an elevation of the Kondo energy. For  $x = 0.05$ , where no magnetic order is detected down to 0.36 K, the  $S_m$  increases smoothly with increasing temperature in a manner consistent with there being strong Kondo hybridization between the  $f$  and conduction electrons. Therefore, it can be assumed that the low temperature side broad feature in  $C_m$  is related to the Kondo effect. For  $x = 1$ , the  $S_m$  at  $T_c$  reaches somewhat higher than the full  $R \ln(2)$ . A possible origin for this is that  $\Delta_{\text{CEF}}$  is small, which can lead to an interplay between the Kondo effect and the CEF splitting. The strong initial increase of  $S_m$  for  $x = 1$  results from a ground state doublet RKKY interaction which is comparable to the Kondo energy scale. The  $S_m(T = T_c)$  data clearly reveals a suppression of the entropy released by the magnetic ordering. This opens the possibility that, while the intersite correlations between  $f$  moments might be reduced by Kondo screening, the Kondo effect dominates and may induce quantum fluctuations at the critical concentration. To estimate the evolution of the Kondo temperature the magnetic entropy is used. It has been observed that the magnetic entropy in many Kondo lattice systems reaches roughly  $0.4\text{--}0.5 R \ln(2)$  at  $T_K$  [28]. The onset temperature where the  $S_m$  reaches  $0.4 R \ln(2)$ , as shown in Fig. 11(c), significantly drops as  $x$  decreases, implying that  $T_K$  decreases with decreasing  $x$ . This observed behavior of  $T_K$  is consistent with the variation of  $C_m/T$  which scales as  $\gamma \propto 1/T_K$  [28].

Interestingly,  $\theta_p^c$  is strongly correlated with the  $T_c$ , whereas  $\theta_p^{ab}$  follows a similar trend as  $T_{\text{max}}^x$  with  $T_{\text{max}}^x \sim \theta_p^{ab}/3$  for the entire  $x$  range (Fig. 12). Since  $\theta_p^c$  follows the phase boundary  $T_c$  as  $x$  decreases,  $\theta_p^c$  promotes the magnetic coupling between  $f$  electrons, indicating the decrease of the RKKY interaction. The correlation between  $T_{\text{max}}^x$  and  $\theta_p^{ab}$  suggests magnetic coupling between  $f$  and conduction electrons in conjunction with the CEF effect. The analysis of the magnetic susceptibility results suggests a strong directional dependence of the exchange interactions. As the RKKY interaction is mediated by the conduction electrons an anisotropic band structure may cause a directional dependence.

Figure 11(d) shows the  $x$  dependence of the  $C_m/T$  value at  $T = 1.8$  K for  $x \geq 0.4$  and at  $T = 0.4$  K for  $0.05 \leq x \leq 0.3$ .

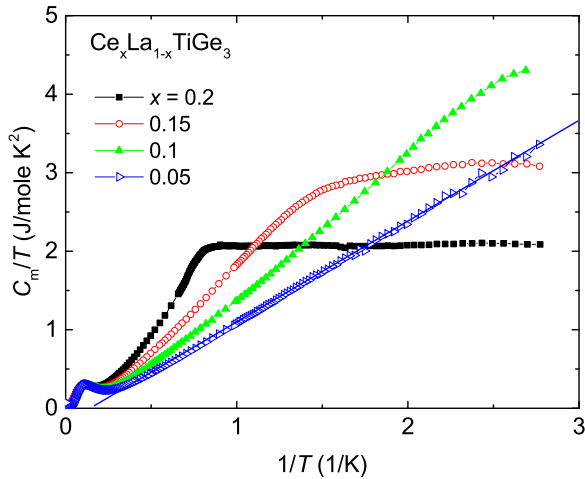


FIG. 14.  $C_m/T$  of  $Ce_xLa_{1-x}TiGe_3$  for  $x = 0.2, 0.15, 0.1,$  and  $0.05$ , plotted as a function of  $1/T$ . Solid line is guide to the eye.

The  $C_m/T$  sharply increases as  $x$  decreases and shows a maximum at  $x_c$ , which indicates that the effective mass diverges close to the critical concentration  $x_c$ . Note that due to the magnetic ordering ( $x \geq 0.15$ ) and single ion Kondo effect the  $T^2$  coefficient of the electrical resistivity can't be reliably estimated, and thus the Kadowaki-Wood ratio was not estimated. The ferromagnetism of  $CeTiGe_3$  is linearly suppressed with decreasing  $x$  and vanished around  $x_c$ . The Hertz-Millis-Moriya (HMM) spin fluctuation theory [39–41] predicts for the dependence of  $T_c$  on the control parameter  $x$  tuning the ferromagnetism toward the QCP,  $T_c(x) = (x - x_c)^\mu$ , where the critical exponent  $\mu = 3/4$  and  $\mu = 1$  for a FM QCP in three dimensions (3D) and two dimensions (2D) [3], respectively. The  $x$ - $T$  phase diagram for  $Ce_xLa_{1-x}TiGe_3$  reveals that  $T_c(x)$  is compatible with  $\mu = 1$  and  $x_c = 0.1$ . Since the magnetization measurements clearly show the very large anisotropy between  $H \parallel ab$  and  $H \parallel c$ , two dimensionality of magnetic fluctuations might arise from exchange anisotropies. Although the phase diagram is compatible with 2D FM spin fluctuations, the power-law dependence of the  $C_m/T$  close to the critical concentration is different from the expected temperature dependence,  $C_m/T \propto T^{-1/3}$ , for the 2D FM fluctuations [3]. To identify the effect of FM fluctuations in this system it is necessary to perform microscopic measurements such as NMR, neutron scattering, and  $\mu$ SR.

The physical properties of many heavy fermion metals indicate a non-Fermi liquid behavior close to the QCP as a signature of quantum fluctuations. The specific heat coefficient generally follows  $C/T \propto -\log(T)$  or  $C/T \propto T^{-\lambda}$  with  $\lambda < 1$  and the electrical resistivity obeys  $\rho = \rho_0 + AT^n$  with  $n < 2$  [3,4,42–44]. It has been observed that the suppression of ferromagnetism toward  $T \rightarrow 0$  leads to various ground state phase diagrams such as tricritical wings, quantum Griffiths phase, and non-Fermi liquid behavior [9]. For the  $Ce_xLa_{1-x}TiGe_3$  system, the  $C_m/T$  and  $\rho(T)$  curves close to  $x_c$  do not follow a non-Fermi liquid behavior. The electrical resistivity shows a single ion behavior and interestingly the  $C_m/T$  curves exhibit an approximately power law dependence  $C_m/T \propto T^{-\lambda}$  with  $\lambda \geq 1$  as shown in Fig. 14. The  $C_m/T$  curves are steeply rising as decreasing

temperature and flatten off below  $T_c$  for  $x = 0.2$  and  $x = 0.15$  and crossover into  $C_m/T \propto T^{-\lambda}$  with  $\lambda = 1$  for  $x = 0.05$ . The temperature dependence of  $C_m/T$  is not compatible with the currently proposed theories for FM quantum criticality. The lack of non-Fermi liquid behavior raises an issue that the observed low temperature properties are not related to a classical QCP. When the FM ordering is suppressed by an external pressure, the second order FM transition often becomes the first order close to the putative QCP or the FM QCP is avoided by an emergent modulated magnetic phase [19,45–49]. The electrical resistivity measurements under pressure show that the parent compound  $CeTiGe_3$  avoids the FM QCP due to the appearance of the new magnetic phase around 4.1 GPa. The external magnetic field under pressure above 4.1 GPa induces a wing-structure phase diagram [26]. So far, however, several non-Fermi liquid systems have been found in FM Kondo lattice compounds; such behavior occurred when the  $T_c$  is suppressed by doping [9]. For example, the non-Fermi liquid of  $U_xTh_{1-x}Cu_2Si_2$  occurs beyond where the ferromagnetism is suppressed, so that  $C/T$  behaves as  $-\log(T)$  and the resistivity indicates a linear temperature dependence [50]. Therefore, the possibility of changing the second order FM transition for  $x = 1$  to a first-order or a modulated AFM phase near  $x_c$  must be investigated by further detailed measurements.

The presence of the localized  $f$ -electron spins in the  $Ce_xLa_{1-x}TiGe_3$  system is confirmed from the Curie-Weiss behavior of the  $\chi(T)$  curves at high temperatures. In both dilute and dense Kondo systems, the screening of  $f$  moments by conduction electrons takes place below  $T_K$ . When the temperature is decreased below  $T_K$ , the  $\chi(T)$  is transformed into the temperature-independent Pauli susceptibility with significantly enhanced value, which is inversely proportional to  $T_K$  ( $\chi \propto 1/T_K$ ) for  $T \ll T_K$ . Similarly,  $C_m/T$  increases with decreasing temperature and becomes saturated at a Sommerfeld coefficient  $\gamma$ , which is also inversely proportional to  $T_K$  ( $\gamma \propto 1/T_K$ ) for  $T \ll T_K$ . For  $Ce_xLa_{1-x}TiGe_3$  the very large value of the electronic specific heat coefficient  $\gamma$  is found for low- $x$  regimes, entering the heavy fermion state by reducing the Kondo temperature. The highly enhanced  $C_m/T$  value of nearly 4.3 J/mol K<sup>2</sup> at 0.4 K is found for  $x = 0.1$  and a slightly lower value for  $x = 0.05$ , reflecting a small value of  $T_K$  and an extremely large effective mass of the charge carriers at low temperatures. When the low temperature broad feature observed in  $C_m$  for  $x = 0.05$  and 0.1 is considered to be due to the single ion Kondo effect, it is expected that the  $C_m/T$  curve will saturate at temperatures much lower than 0.4 K. While the Sommerfeld coefficient in a single ion Kondo model always becomes finite in the Fermi liquid for  $T \rightarrow 0$ , one can imagine that the Kondo temperature is too small to observe the flattening in the experimental data for  $x = 0.05$ . In this case, the  $\chi(T)$  curve is also expected to level off at low temperatures. The  $\chi(T)$  for  $H \parallel c$  clearly indicates a power law dependence ( $\chi \propto 1/T$ ) below 10 K as presented in Fig. 3(c). It may be interesting to conduct further experiments down to much lower temperatures to investigate whether both  $C_m/T$  and  $\chi(T)$  diverge as  $1/T$  or saturate with a finite value.

There are multiple, plausible explanations for the power law dependence of  $C_m/T$ . It can be the consequence of the Kondo screening resulting from a dilution of the magnetic

Ce<sup>3+</sup> lattice, where the combined effect of the single ion Kondo and electronic Schottky contribution is accidentally producing  $C_m/T \propto 1/T$ . It can be a consequence of the suppression of the exchange interaction between  $f$  electrons due to the Kondo screening, inducing quantum fluctuations close to the critical concentration, however deviating from the conventional quantum criticality. Another possibility might be the result of the disorder induced by La substitutions, avoiding QCP and forming a quantum Griffiths phase [51,52]. The formation of the quantum Griffiths phase has been reported in doped systems such as Ni<sub>1-x</sub>V<sub>x</sub> [20,21] and CePd<sub>1-x</sub>Rh<sub>x</sub> [53]. Although the magnetization isotherms for  $x = 0.05$  in Ce<sub>x</sub>La<sub>1-x</sub>TiGe<sub>3</sub> clearly indicates dHvA oscillations above 50 kOe, there is a Ce-site disorder by La substitution, which may also form a cluster glass phase or percolation limit. In this case the observed power law dependence of  $C_m/T$  and  $\chi(T)$  behavior may be described by the quantum Griffiths phase scenario, which predicts  $\chi \sim C/T \sim T^{-\lambda}$  with  $0 \leq \lambda \leq 1$ . In this scenario, however, the inhomogeneous suppression of magnetic order causes a development of a tail close to the  $x_c$  in the phase diagram, masking the actual QCP by the formation of the disorder induced phases. In contrast, the tail is absent in Ce<sub>x</sub>La<sub>1-x</sub>TiGe<sub>3</sub> when the  $T_c$  is extrapolated from high- $x$  regime to the  $x_c$ . In addition, although no hysteresis is observed in thermodynamic and transport measurements, a formation of spin-glass state should not be excluded. Further work must be performed to clarify whether the FM QCP is present in Ce<sub>x</sub>La<sub>1-x</sub>TiGe<sub>3</sub> and, if not, whether the QCP is avoided due to the appearance of a new phase induced by disorder.

## V. SUMMARY

In summary, magnetization, specific heat, and electrical resistivity measurements have been performed on single crystalline Ce<sub>x</sub>La<sub>1-x</sub>TiGe<sub>3</sub> systems. The  $x$ - $T$  phase diagram has been constructed, where the ferromagnetic order is linearly suppressed to  $T = 0$  at the critical concentration  $x_c \sim 0.1$  at which both the specific heat coefficient  $C_m/T$  and susceptibility  $\chi(T)$  follow a power law behavior. A transition from Kondo lattice for  $x = 1$  to single ion behavior for  $x = 0.05$  is observed from the electrical resistivity measurements. The very large value of  $C_m/T$  can be achieved by partially replacing La by Ce ions. All samples in this study exhibit strong magnetic anisotropies, which is mostly due to crystalline electric field effects. The compounds in this series appear to be Kondo lattice systems with varying energy scales of Kondo and RKKY interaction and crystalline electric field. These energy scales can be effectively inferred from the experimental observations of local maxima developed in thermodynamic and transport properties. The lack of non-Fermi liquid behavior excludes a standard quantum critical point in Ce<sub>x</sub>La<sub>1-x</sub>TiGe<sub>3</sub> and raises the question about the origin of the anomalous low temperature behavior.

## ACKNOWLEDGMENTS

This work was supported by the Canada Research Chairs program, the Natural Science and Engineering Research Council of Canada, and the Canadian Foundation for Innovation.

- 
- [1] G. R. Stewart, *Rev. Mod. Phys.* **56**, 755 (1984).  
 [2] S. Doniach, *Physica B* **91**, 231 (1977).  
 [3] G. R. Stewart, *Rev. Mod. Phys.* **73**, 797 (2001); **78**, 743 (2006).  
 [4] H. von Löhneysen, A. Rosch, M. Vojta, and P. Wölfle, *Rev. Mod. Phys.* **79**, 1015 (2007).  
 [5] P. Gegenwart, Q. Si, and F. Steglich, *Nat. Phys.* **4**, 186 (2008).  
 [6] S. Sachdev, *Phys. World* **12**, 33 (1999).  
 [7] Q. Si, *Phys. Status Solidi B* **247**, 476 (2010).  
 [8] P. Coleman, *Phys. Status Solidi B* **247**, 506 (2010).  
 [9] M. Brando, D. Belitz, F. M. Grosche, and T. R. Kirkpatrick, *Rev. Mod. Phys.* **88**, 025006 (2016).  
 [10] B. J. Holt, J. D. Ramsden, H. H. Sample, and J. G. Huber, *Physica B+C* **107**, 255 (1981).  
 [11] K. D. Myers, S. L. Bud'ko, I. R. Fisher, Z. Islam, H. Kleinke, A. H. Lacerda, and P. C. Canfield, *J. Magn. Magn. Mater.* **205**, 27 (1999).  
 [12] S. K. Malik and D. T. Adroja, *Phys. Rev. B* **43**, 6295(R) (1991).  
 [13] P. Manfrinetti, S. Dhar, R. Kulkarni, and A. Morozkin, *Solid State Commun.* **135**, 444 (2005).  
 [14] N. Tsujii, L. Keller, A. Dönni, and H. Kitazawa, *J. Phys.: Condens. Matter* **28**, 336002 (2016).  
 [15] A. Steppke, R. Küchler, S. Lausberg, E. Lengyel, L. Steinke, R. Borth, T. Lühmann, C. Krellner, M. Nicklas, C. Geibel, F. Steglich, and M. Brando, *Science* **339**, 933 (2013).  
 [16] A. Huxley, I. Sheikin, E. Ressouche, N. Kernavanois, D. Braithwaite, R. Calemczuk, and J. Flouquet, *Phys. Rev. B* **63**, 144519 (2001).  
 [17] S. Araki, M. Hayashida, N. Nishiumi, H. Manabe, Y. Ikeda, T. C. Kobayashi, K. Murata, Y. Inada, P. Wiśniewski, D. Aoki, Y. Ōnuki, E. Yamamoto, and Y. Haga, *J. Phys. Soc. Jpn.* **84**, 024705 (2015).  
 [18] D. Aoki, A. Huxley, E. Ressouche, D. Braithwaite, J. Flouquet, J. Brison, E. Lhotel, and C. Paulsen, *Nature (London)* **413**, 613 (2001).  
 [19] V. Taufour, D. Aoki, G. Knebel, and J. Flouquet, *Phys. Rev. Lett.* **105**, 217201 (2010).  
 [20] S. Ubaid-Kassis, T. Vojta, and A. Schroeder, *Phys. Rev. Lett.* **104**, 066402 (2010).  
 [21] R. Wang, A. Gebretsadik, S. Ubaid-Kassis, A. Schroeder, T. Vojta, P. J. Baker, F. L. Pratt, S. J. Blundell, T. Lancaster, I. Franke, J. S. Möller, and K. Page, *Phys. Rev. Lett.* **118**, 267202 (2017).  
 [22] C. Pfeleiderer, S. R. Julian, and G. G. Lonzarich, *Nature (London)* **414**, 427 (2001).  
 [23] A. V. Morozkin, *J. Alloys Compd.* **370**, L1 (2004).  
 [24] W. Kittler, V. Fritsch, F. Weber, G. Fischer, D. Lamago, G. André, and H. v. Löhneysen, *Phys. Rev. B* **88**, 165123 (2013).  
 [25] M. Inamdar, A. Thamizhavel, and S. K. Dhar, *J. Phys.: Condens. Matter* **26**, 326003 (2014).

- [26] U. S. Kaluarachchi, V. Taufour, S. L. Bud'ko, and P. C. Canfield, *Phys. Rev. B* **97**, 045139 (2018).
- [27] R. Khan, J. Yang, H. Wang, Q. Mao, J. Du, B. Xu, Y. Zhou, Y. Zhang, B. Chen, and M. Fang, *Mater. Res. Express* **3**, 106101 (2016).
- [28] A. C. Hewson, *The Kondo Problem to Heavy Fermions* (Cambridge University Press, Cambridge, 1997).
- [29] V. T. Rajan, *Phys. Rev. Lett.* **51**, 308 (1983).
- [30] H. Yashima, T. Satoh, H. Mori, D. Watanabe, and T. Ohtsuka, *Solid State Commun.* **41**, 1 (1982).
- [31] C. L. Lin, T. Yuen, P. Riseborough, X.-Y. Huang, and J. Li, *J. Appl. Phys.* **91**, 8117 (2002).
- [32] S. L. Bud'ko, H. Hodovanets, A. Panchula, R. Prozorov, and P. C. Canfield, *J. Phys.: Condens. Matter* **26**, 146005 (2014).
- [33] K. G. Wilson, *Rev. Mod. Phys.* **47**, 773 (1975).
- [34] D. Andreica, K. Alami-Yadri, D. Jaccard, A. Amato, and D. Schenck, *Physica B* **259-261**, 144 (1999).
- [35] D. Huo, J. Sakurai, O. Maruyama, T. Kuwai, and Y. Isikawa, *J. Magn. Magn. Mater.* **226-230**, 202 (2001).
- [36] U. Köhler, N. Oeschler, F. Steglich, S. Maquilon, and Z. Fisk, *Phys. Rev. B* **77**, 104412 (2008).
- [37] E. D. Mun, S. Jia, S. L. Bud'ko, and P. C. Canfield, *Phys. Rev. B* **86**, 115110 (2012).
- [38] H.-U. Desgranges and J. W. Rasul, *Phys. Rev. B* **32**, 6100 (1985).
- [39] J. A. Hertz, *Phys. Rev. B* **14**, 1165 (1976).
- [40] A. J. Millis, *Phys. Rev. B* **48**, 7183 (1993).
- [41] T. Moriya and T. Takimoto, *J. Phys. Soc. Jpn.* **64**, 960 (1995).
- [42] H. von Löhneysen, *J. Phys.: Condens. Matter* **8**, 9689 (1996).
- [43] D. Belitz, T. R. Kirkpatrick, and T. Vojta, *Rev. Mod. Phys.* **77**, 579 (2005).
- [44] R. P. Smith, M. Sutherland, G. G. Lonzarich, S. S. Saxena, N. Kimura, S. Takashima, M. Nohara, and H. Takagi, *Nature (London)* **455**, 1220 (2008).
- [45] D. Belitz, T. R. Kirkpatrick, and T. Vojta, *Phys. Rev. B* **55**, 9452 (1997).
- [46] D. Belitz, T. R. Kirkpatrick, and T. Vojta, *Phys. Rev. Lett.* **82**, 4707 (1999).
- [47] A. V. Chubukov, C. Pépin, and J. Rech, *Phys. Rev. Lett.* **92**, 147003 (2004).
- [48] H. Kotegawa, T. Toyama, S. Kitagawa, H. Tou, R. Yamauchi, E. Matsuoka, and H. Sugawara, *J. Phys. Soc. Jpn.* **82**, 123711 (2013).
- [49] V. Taufour, U. S. Kaluarachchi, R. Khasanov, M. C. Nguyen, Z. Guguchia, P. K. Biswas, P. Bonfà, R. De Renzi, X. Lin, S. K. Kim, E. D. Mun, H. Kim, Y. Furukawa, C.-Z. Wang, K.-M. Ho, S. L. Bud'ko, and P. C. Canfield, *Phys. Rev. Lett.* **117**, 037207 (2016).
- [50] M. Lenkewitz, S. Corsépius, G.-F. V. Blanckenhagen, and G. R. Stewart, *Phys. Rev. B* **55**, 6409 (1997).
- [51] J. A. Hoyos, C. Kotabage, and T. Vojta, *Phys. Rev. Lett.* **99**, 230601 (2007).
- [52] T. Vojta, C. Kotabage, and J. A. Hoyos, *Phys. Rev. B* **79**, 024401 (2009).
- [53] M. Brando, T. Westerkamp, M. Deppe, P. Gegenwart, C. Geibel, and F. Steglich, *J. Phys.: Conf. Ser.* **200**, 012016 (2010).